論文 80-17-1-4

Modifcation of Reconstruction Filter for Low-Dose Reconstruction

(低照射光 再構成을 위한 필터 設計)

廉 泳 鎬 *

(Yum, Young - Ho)

要 約

C. T. (電算化 斷層 映像 處理) 映像再構成의 경우, 投射되는 光量子 (X-ray, positron 등)가 적을 때는 雜音에 의한 효과가 增幅되어 再構成된 画面은 거의 알아 볼 수 없게 된다. 그 경우 画質을 높이기 위해서는 再構成 필터를 射影 데이터 (projection data)의 信號對雜音比에 따라 修正시켜야 할 필요성이 생긴다. 이 논문에서는 射影 데이터에서 얻은 情報를 사용하여 再構成 필터를 修正하는 方法에 관하여 考察하고 그에 대한 시뮬레이션을 행하였다. 시뮬레이션의 결과, 이 方法은 再構成 画像에서의 雜音을 줄여, 그 分解能力을 크게 向上시킬 수 있음이 判明되었다. 또한 이 필터를 近似的으로 具現하는 方法에 관하여도 논하고, 그 近似 필터의 回歸的 構成 (recursive implementation)의 가능성에 관하여도 言及하였다.

Abstract

The reconstruction problem in a low dose case requires some compromise of resolution and noise artifacts, and also some modification of filter kernels depending on the signal-to-noise ratio of projection data. In this paper, an algorithm for the reconstruction of an image function from noisy projection data is suggested, based on minimum-mean-square error criterion. Modification of the filter kernel is made from information (statistics) obtained from the projection data. The simulation study proves that this algorithm, based on the Wiener filter approach, provides substantially improved image with reduction of noise as well as improvement of the resolution. An approximate method was also studied which leads to the possible use of a recursive filter in the convolution process of image reconstruction.

I. Introduction

The deblur function for the convolution-back projection technique is of well-known form[1]

$$\phi(\omega) = \begin{cases} |\omega|, & |\omega| \leq \Omega \\ 0, & |\omega| > \Omega \end{cases} \quad \cdots\cdots\cdots\cdots (1)$$

where Ω should be larger than the bandwidth of the image to be reconstructed. This filter function of Ramachandran and Lakshminarayanan[1] with linear interpolation in back projection provides good reconstructed image for high signal-to-noise ratio. As is known, it is sensitive to noise. Shepp and Logan[2] developed a filter with less sensitivity to noise and this has also less ringing artifacts at edge of the image with only minor loss of sharpness. Recently, Tsui

* 正會員, 韓國科學院 電氣 및 電子工學科
(Dept. of Electrical Science, KAIS)

接受日字: 1979年 11月 2日

and Budinger[3] proposed non-stationary deblur function for low dose reconstruction. In this paper, we will consider the formation of stationary deblur function.

As mentioned above, there is a need for a trade-off between resolution and noise. It depends on the application situation. The general form of the reconstruction filter can be written as

$$\phi(\omega) = |\omega| \; H(\omega, \theta) \quad \cdots\cdots (2)$$

where $H(\omega, \theta)$ is an apodizing function. In this paper the problem of minimum-mean-square error will be considered. For the image, minimum-mean-square error criterion can be achieved with well-known Wiener-filter.[4, 5]

$$H(\omega, \theta) = \frac{H_1^*(\omega, \theta)\, \psi_o(\omega, \theta)}{|H_1(\omega, \theta)|^2\, \psi_o(\omega, \theta) + \psi_n(\omega, \theta)} \quad \cdots\cdots (3)$$

where ω and θ are spatial frequencies of image in polar coordinate, $H_1(\omega, \theta)$ is transfer function of sampling process, $\psi_o(\omega, \theta)$ is power spectral density of image, and $\psi_n(\omega, \theta)$ is noise power spectral density function. The concept of filtering the projection data with 2-D Wiener filter was first suggested by Cho and Burger.[6] Their method needs more than two reconstructions and requires estimation of power spectra of image and noise from the noisy reconstruction image. Recent work of Tsui and Budinger[3] utilizes the projection data for the power spectra estimation. They use different filter functions at each projection. A slightly different approach is to construct a filter function from data of the first few projections and use this filter function for filtering successive projection data. With this method, considerable computation time can be saved and some statistical advantage can be gained in some noisy image reconstruction, e.g. in nuclear medicine CT where poor signal-to-noise ratio might require different type of filter kernel than conventional ones.

II. Filter Implementation

The minimum-mean-square-error filter for reconstruction from the projection data is of the form[3]

$$\phi(\omega, \theta) = \frac{|\omega| H_1^*(\omega, \theta)}{|H_1(\omega, \theta)|^2 + \frac{|\omega|}{2\pi} V_p / \psi_o(\omega, \theta)} \quad \cdots\cdots (4)$$

where V_p is the average variance of projection noise. Eq.(4) is a slightly modified form of Eq.(3) for the transverse section reconstruction, i.e. the noise power spectrum is replaced by $\frac{|\omega|}{2\pi} V_p$. In the case of r^{-1} deblurring of stationary independent projection noise, the noise power spectrum is the variance of projection data multiplied by the absolute value of spatial frequency.[7]

In our filter implementation, a Markov field is assumed. The assumption of 2-dimensional Markov field has been widely used in digital image processing (restoration and compression).[8-11] The auto-covariance function for the 2-dimensional Markov process is[5]

$$K(x, y) = R_o \exp\left[-\alpha (x^2 + y^2)^{1/2}\right] \quad \cdots\cdots (5)$$

where R_o is an energy scaling constant and α is a scaling constant. Sometimes we refer to $\rho = \exp(-\alpha)$ as a correlation coefficient. The corresponding power spectrum is

$$\psi_o(\omega_x, \omega_y) = \frac{2\pi \alpha R_o}{(\alpha^2 + \omega_x^2 + \omega_y^2)^{3/2}} \quad \cdots\cdots (6)$$

where $\omega_x^2 + \omega_y^2 = \omega^2$ (for more details, refer to Appendix). As a simplifying assumption, the Markov process is assumed to be of seperable form with an autocovariance function

$$K_1(x, y) = R_o \exp\left[-\alpha_1 |x| - |y|\right]. \quad \cdots\cdots (7)$$

The projection procedure can be easily modeled by Eq.(7), but the filter implemented with Eq.(7) is different at each projection direction, i.e. non-stationary. As a consequence the image parameters R_o, α_1 were estimated using Eq.(7) and the filter is implemented with Eq.(5).

The projection data are the weighted sums (or integrals) of image function (density). So we can assume that the noise of projection data be the sum of distributed noise. With this assumption, some

correlation occurrs between the noise of projection data as shown in Fig. 1. But if sampling width is

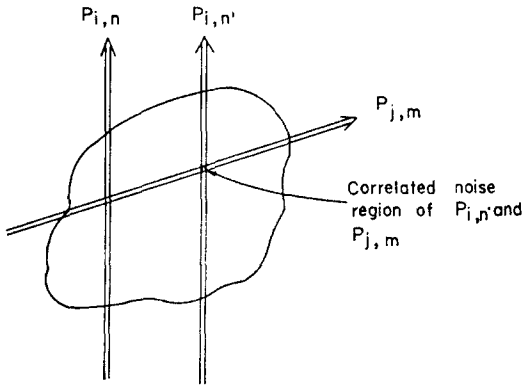

Fig. 1. Correlation of Noise.

small compared with the image size, this correlation is small enough to be neglected. The noisy projection data is given by

$$P_{i,n} = \int_0^{\ell} \int_{x_n - \frac{\Delta}{2}}^{x_n + \frac{\Delta}{2}} [\,0(x,y) + \epsilon(x,y)\,]\, dx\, dy \quad \cdots\cdots (8)$$

where $0(x, y)$ is image function, Δ is detector size, ℓ is projection length, and $\epsilon(x, y)$ is noise. Let us assume that the image function $0(x, y)$ has some constant mean and the variation term, i.e.

$$0(x, y) = I + a(x, y) \quad \cdots\cdots (9)$$

where I is image mean value. Then the Markov assumption of Eq.(7) gives

$$E[\,a(x,y)\, a(x',y')\,] = R_0 \exp[-\alpha_1 |x-x'| - \alpha_1 |y-y'|]. \quad \cdots\cdots (10)$$

Assuming no correlation between image and noise functions, Eq.(8) and Eq.(10) give

$$E[P_{i,n}^2] = I^2 \Delta^2 \ell^2 + R_0 F(\alpha_1) + V_p \quad \cdots\cdots (11)$$

$$E[P_{i,n} P_{i,n+k}] = I^2 \Delta^2 \ell^2 + R_0 \exp(-\alpha_1 kb) G(\alpha_1) \quad \cdots\cdots (12)$$

where

$$F(\alpha_1) = \frac{4}{\alpha_1^2}\left[\,\Delta - \frac{1}{\alpha_1}[\,1 - \exp(-\alpha_1 \Delta)\,]\,\right] \left[\,\ell - \frac{1}{\alpha_1}[\,1 - \exp(-\alpha_1 \ell)\,]\,\right] \quad \cdots\cdots (13)$$

$$G(\alpha_1) = \frac{2}{\alpha_1^2}[\exp(\alpha_1 \Delta) + \exp(-\alpha_1 \Delta) - 2] \left[\,\ell - \frac{1}{\alpha_1}[\,1 - \exp(-\alpha_1 \ell)\,]\,\right] \quad \cdots\cdots (14)$$

and b is the sampling interval. Rearranging Eq.(12), we have

$$\exp(-\alpha_1 b) = \frac{E[P_{i,n}P_{i,n+2}] - I^2 \Delta^2 \ell^2}{E[P_{i,n}P_{i,n+1}] - I^2 \Delta^2 \ell^2} = \frac{E[P_{i,n}P_{i,n+3}] - I^2 \Delta^2 \ell^2}{E[P_{i,n}P_{i,n+2}] - I^2 \Delta^2 \ell^2} \quad \cdots\cdots (15)$$

$$\vdots \quad \vdots$$

And when $\alpha_1 \Delta \ll 1$ as the real case, we can see that

$$G(\alpha_1) \simeq F(\alpha_1). \quad \cdots\cdots (16)$$

From Eqs.(11)-(16), we can see that the projection data is also Markov process if the image field is Markovian. To implement a symmetric filter function, Eq.(7) is fitted to Eq.(5). The best fitting is achieved when

$$\alpha = \sqrt{2}\ \alpha_1. \quad \cdots\cdots (17)$$

Using Eq.(11)-(17), the image coefficients R_0, α can be estimated from the projection data.

Then the minimum-mean-square-error filter is given by

$$\phi(\omega) = \frac{|\omega|}{1 + \gamma \dfrac{|\omega| V_p}{4\pi^2 \alpha R_0} (\alpha^2 + \omega^2)^{3/2}} \quad \cdots\cdots (18)$$

where only noise filtering is considered and transfer function of the detector blur is assumed unity, and γ is a factor to prevent over-smoothing of reconstructed image.

Let us consider an approximate implementation of Eq.(18). Usually α is very small, and we can approximate Eq.(18) as

$$\phi(\omega) = \frac{|\omega| \beta^4}{\omega^4 + \beta^4} \quad \cdots\cdots (19)$$

where β^4 is given by

$$\beta^4 = \frac{4\pi^2 \alpha R_0}{V_p \gamma} \quad \cdots\cdots (20)$$

And R_0 is given by

$$R_0 = \frac{E[P_{i,n}^2] - m^2 - V_p}{F(\alpha_1)} \quad \cdots\cdots (21)$$

where m is the mean value of projection data and $F(\alpha_1)$ is given by Eq.(13). When $\alpha_1 \Delta \ll 1$, Eq.(13) becomes

$$F(\alpha_1) \simeq \frac{2}{\alpha_1}\left[\ell - \frac{1}{\alpha_1}[1-\exp(-\alpha_1 \ell)]\right] \cdots\cdots (22)$$

When ℓ is sufficiently large, Eq.(22) can be approximated as

$$F(\alpha_1) \simeq \frac{2}{\alpha_1}\left(\ell - \frac{1}{\alpha_1}\right). \quad \cdots\cdots (23)$$

Then Eq.(20) becomes

$$\beta^4 = \frac{2\sqrt{2}\,\pi^2\,\alpha_1^3}{\gamma V_p} \frac{E[P_{1,n}^2] - m^2 - V_p}{\alpha_1 - \ell} \quad \cdots\cdots (24)$$

Usually the correlation of projection data is large, and α_1 is 0.02-0.06, when the sampling interval is normalized to unity. Then Eq.(24) is approximated as

$$\beta^4 = \frac{0.07\,\Gamma}{0.05M - 1} S \quad \cdots\cdots (25)$$

where M is number of rays per projection, α_1 is set 0.05, γ is set 0.05, and Γ is a multiplication factor. And S is effective SNR of projection data, which is given by

$$S = \frac{E[P_{i,n}^2] - m^2 - V_p}{V_p}. \quad \cdots\cdots (26)$$

where the numerator is the r.m.s. value of projection data. In Eq.(25) M is used instead of ℓ, because the projection length ℓ can be approximated as the number of samples in each projection when the sampling interval is normalized.

One interesting aspect of Eq.(19) is that the filter can be easily implemented with recursive form using well-known impulse invariant transform[12] when β^4 is small, i.e. the noise is high. In recursive implementation, two recursions are required, i.e. forward and backward, to get the zero phase condition. The condition for the recursive filtering is given by

$$\beta^4 \leqslant 0.31 \quad \cdots\cdots (27)$$

i.e.

$$\Gamma S \leqslant 0.2214\,M - 4.429 \quad \cdots\cdots (28)$$

where the critical value of β^4 is chosen such that the frequency response at $\omega = \frac{\pi}{b}$ is -40 dB.

In convolution - back projection algorithm, the main burden of computation is back projection. The computation saving with recursive filtering, therefore, is not so large but still appreciable. The use of recursive filter may appear useful in some cases.

III. Results of Simulation

In simulation, the exact form of Eq.(18) was used, and γ was taken to be 0.05. The algorithm was implemented by following steps;

1. Get projection data, add noise, and write in data file.
2. Read a few projection data and estimate image parameters.
3. Construct Wiener filter.
4. Read the first projection data.
5. Perform FFT of projection data.
6. Multiply the results of step #3 and those of step #5.
7. Perform inverse FFT.
8. Back-project.
9. Read next projection data and start at step #5.

In the above filter implementation, the frequency sampling technique[12] was used. To smooth the truncation effect,[5] the sampled frequency response was inverse-transformed and windowed with some window function,[12] which can be chosen by input parameter in the program, and then it was re-transformed.

Phantom used for the simulation is shown in Fig. 2. The left-sided numbers are diameters of circles in units of pixel when the image size is 64 x 64 pixels. The diameter of the large circle is 60 pixels. We used two simulation phantoms of same shape but of different contrast. The lower-sided numbers are the contrast of two phantoms, where the contrasts are

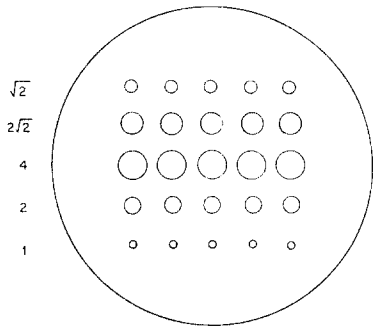

LOW CONTRAST	1.02	1.10	1.20	1.05	1.01
HIGH CONTRAST	1.10	1.50	2.00	1.20	1.05

Fig. 2. Phantom used for the simulation. The left sided numbers are diameters of circles in pixel units, when the image size is 64 pixels X 64 pixels. The lower-sided numbers are contrasts of circles in two phantoms.

defined as (signal level)/(background). The density of the large circle was set to unity.

In simulation, the projection is approximated by the strip integral. For each projection data, the noise, the variance of which is proportional to projection data, is added. The noise standard deviations are 0.45%, 1.4%, and 4.5% of square roots of projection data, respectively. For high contrast phantom, simulation is also performed with noise standard deviation of 14.1% of square root of projection data. In simulation, the projection data are sampled at 128 points and 256-point FFT is performed, for 64 x 64 reconstructed images. For comparison, the reconstructions are also performed using Shepp and Logan's

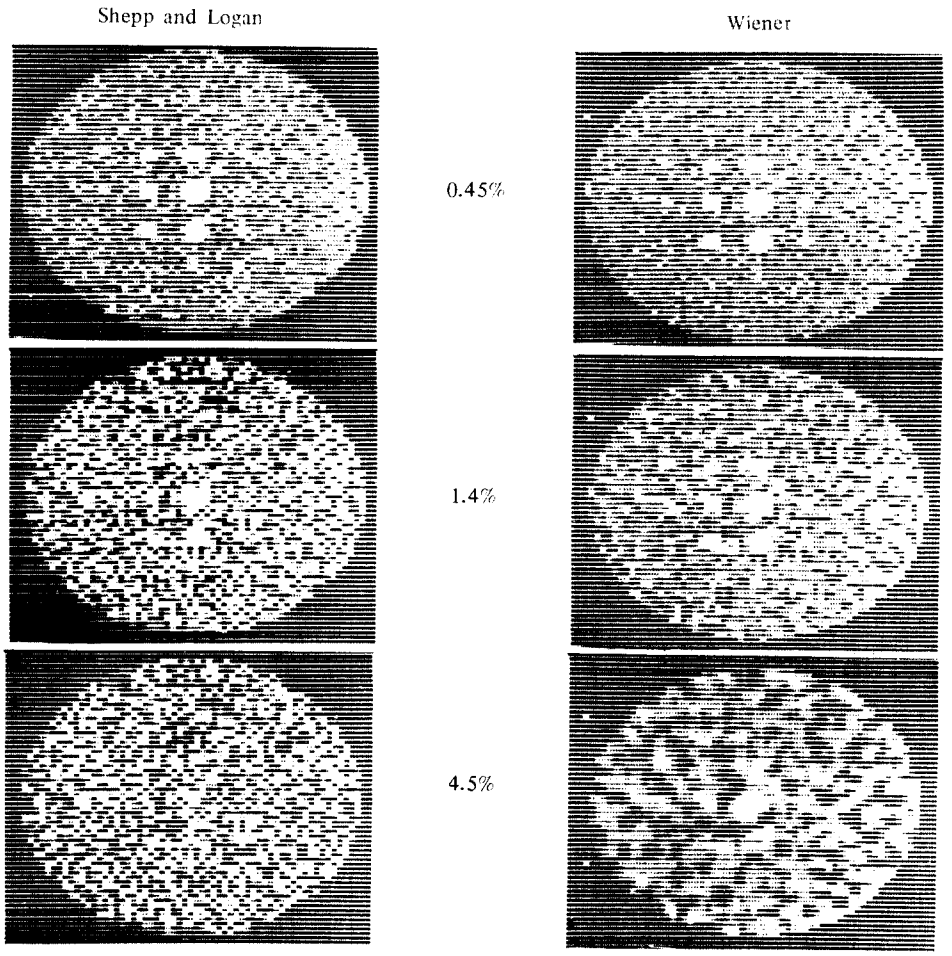

Fig. 3. Reconstructed images of low contrast phantom. The numbers represent the quantity of noise. The noise standard deviations are the numbers multiplied by square roots of projection data. The images are recon structed using 100 views over π and 128 samples per each view.

algorithm. The Shepp and Logan's filtering was carried out in spatial domain via discrete convolutions. In both cases, the linear interpolation is adopted for back projection.

The simulated results are shown in Fig. 3 for low contrast phantom, and in Fig. 4 for high contrast phantom. To observe the fine details of reconstructed images, grey levels are sliced at suitable levels. For the comparison of two pictures, same dynamic range of grey levels are used.

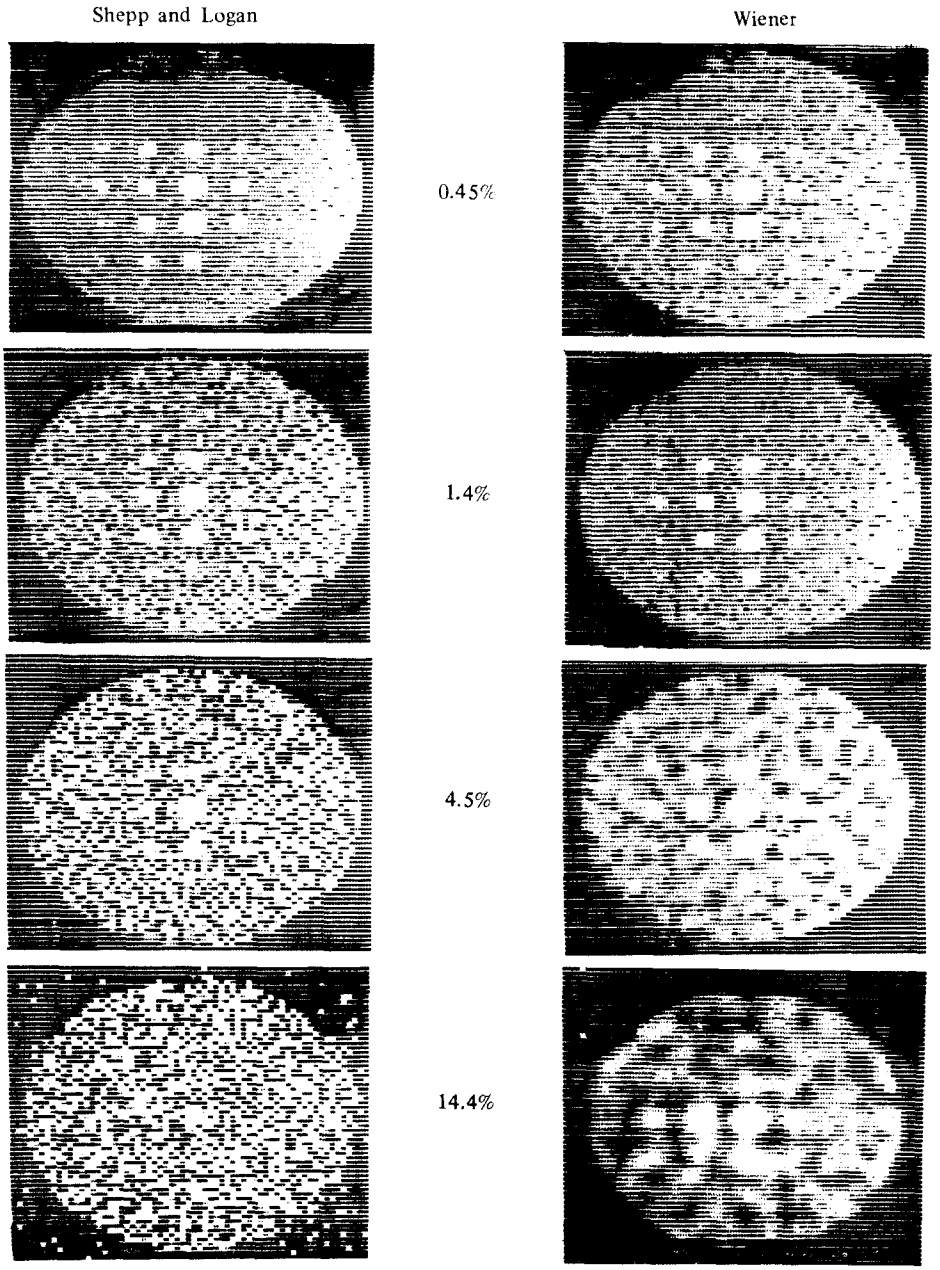

Fig. 4. Reconstructed images of high contrast phantom. The numbers represent the quantity of noise. The noise standard deviations are the numbers multiplied by square roots of projection data. The images are reconstructed using 100 views over π and 128 samples per each view.

IV. Conclusions and Discussion

One possible way to filter noise has been shown in the reconstruction problem based on minimum-mean square-error sense. As can be seen from the simulation results, the filtering effect is promising when compared with the unfiltered versions. Up to 4.5% noise, the Wiener filter approach gives considerable resolution improvement. An approximate method was also given as well as the possible use of a recursive filter. As mentioned above, some saving of computation time with recursive filter implementation can be seen.

It should be mentioned also that the minimum-mean-square error is not always an optimum criterion for all the applications. Sometimes more noise can be endured with other techniques, if noise and resolution can be compromised. More study is needed on these points.

Our study was limited to noise filtering of convolution – back projection algorithm. For optimum noise filtering, the direct Fourier transform technique[13] can also be efficient, since this method does not require back projection. In this case, the image and noise power spectra can easily be estimated directly from the reconstructed image, and using this information conventional two-dimensional image restoration can easily be performed.

Appendix

Power Spectrum of 2-Dimensional Markov Process

The power spectrum of a stationary image is defined as 2-dimensional Fourier transform of its auto-covariance function. The Fourier transform of Eq.(5) is

$$\psi_0(\omega_X,\omega_Y) = \iint_{-\infty}^{\infty} R_0 \exp[-\alpha(x^2 + y^2)^{1/2}] \exp[-j(\omega_X x + \omega_Y y)]\, dxdy \quad \cdots (A\text{-}1)$$

where $j = \sqrt{-1}$. Making transform to polar coordinates in both x – y plane and ω_X – ω_Y plane, i.e.

$$\left.\begin{aligned} x &= r\cos\varphi \\ y &= r\sin\varphi \\ r &= \sqrt{x^2 + y^2} \\ \varphi &= \tan^{-1}\left(\frac{x}{y}\right) \end{aligned}\right\} \quad \cdots\cdots (A\text{-}2)$$

$$\left.\begin{aligned} \omega_X &= \omega\cos\theta \\ \omega_Y &= \omega\sin\theta \\ \omega &= \sqrt{\omega_X^2 + \omega_Y^2} \\ \theta &= \tan^{-1}\left(\frac{\omega_X}{\omega_Y}\right) \end{aligned}\right\}, \quad \cdots\cdots (A\text{-}3)$$

we have

$$\psi_0(\omega,\theta) = \int_0^{\infty}\int_0^{2\pi} R_0 r \exp(-\alpha r) \exp[-j\omega r\cos(\varphi-\theta)]\, d\varphi dr. \quad \cdots\cdots (A\text{-}4)$$

Using the Bessel function identity

$$J_0(a) = \frac{1}{2\pi}\int_0^{2\pi} \exp[-ja\cos(\varphi-\theta)]\, d\varphi \quad \cdots\cdots (A\text{-}5)$$

where $J_0(\cdot)$ is the zero-order Bessel function of the first kind, then Eq. (A-4) becomes

$$\psi_0(\omega) = 2\pi R_0 \int_0^{\infty} r \exp(-\alpha r)\, J_0(\omega r)\, dr \quad \cdots\cdots (A\text{-}6)$$

where the angle θ is omitted, because the dependence of the transform on angle θ disappears. R.H.S. of Eq. (A-6) is the zero-order Hankel transform of $2\pi R_0 \exp(-\alpha r)$, which is given by[14]

$$\psi_0(\omega) = \frac{2\pi\alpha R_0}{(\alpha^2 + \omega^2)^{3/2}} \quad \cdots\cdots (A\text{-}7)$$

Substituting Eq. (A-3) in Eq. (A-7), we have Eq. (6).

Acknowledgement

The author would like to express his sincere gratitute to Dr. Zang-Hee Cho for his grateful suggestions and guidance. The author is also indebted to the reviewers, who made many helpful suggestions to improve this paper.

References

1. G. Ramachandran and A. Lakshminarayanan; "Three-Dimensional Reconstruction from Radiographs and Electron Micrographs: Application of Convolution Instead of Fourier Transforms," Proc. Nat. Acad. Sci. USA, Vol. 68, pp 2236-2240, 1971.
2. L. Shepp and B. Logan; "The Fourier Reconstruction of a Head Section," IEEE Trans. Nucl. Sci., Vol. NS-21, pp 21-43, June 1974.
3. E.T. Tsui and T.F. Budinger; "A Stochastic Filter for Transverse Section Reconstruction," IEEE Trans. Nucl. Sci., Vol. NS-26, pp 2687-2690, April 1979.
4. H.C. Andrews and B.R. Hunt; Digital Image Restoration, Pretice-Hall, Englewood Cliffs, N.J., 1977.
5. W.K. Pratt; Digital Image Processing, Wiley-Interscience, New York, N.Y., 1978.
6. Z.H. Cho and J.R. Burger; "Construction, Restoration, and Enhancement of 2 and 3-Dimensional Images," IEEE Trans. Nucl. Sci., Vol. NS-24, pp 886-899, April 1977.
7. J.P. Stonestrom and R.E. Alvarez; "Optimal Processing of Compted Tomography Images," Proc. Int. Opt. Computing Conf. '77, in Application of Digital Image Processing, SPIE Vol. 119, Soc. Photo-Optical Instr. Engin., Bellingham, Wash., 1977.
8. A. Habibi; "Two-Dimensional Baysian Estimate of Images," Proc. IEEE, Vol. 60, pp 878-883, July 1972.
9. A.K. Jain and E. Angel; "Image Restoration, Modeling, and Reduction of Dimensionality," IEEE Trans. Compt. Vol. C-23, pp 470-476, May 1974.
10. D.P. Panda and A.C. Kak; "Recursive Least Square Smoothing of Noise in Images," IEEE Trans. Acous. Speech Sig. Proc., Vol. ASSP-25, pp 520-524, December 1977.
11. J.W. Wood; "Markov Image Modeling," IEEE Trans. Automat. Contr., Vol. AC-23, pp 846-850, October 1978.
12. A.V. Oppenheim and R.W. Schafer; Digital Signal Processing, Prentice-Hall, Englewood Cliffs, N.J., 1975.
13. R.M. Mersereau; "Direct Fourier Transform Techniques in 3-D Image Reconstruction," Computers in Biology and Medicine, Vol. 6, pp 247-258, October 1976.
14. I.N. Sneddon; The Use of Integral Transform, McGraw-Hill, New York, N.Y., 1972.